Published in final edited form as:

Noise Control Eng J. 2011 November 1; 59(6): 591–612. doi:10.3397/1.3659660.

Development of elastomeric isolators to reduce roof bolting machine drilling noise

Robert Michael[a], **David Yantek**[b], **David Johnson**[c], **Ernie Ferro**[d], and **Chad Swope**[e]

[a] Penn State Erie, The Behrend College, School of Engineering, 5101 Jordan Road, Erie, PA, 16563 USA; rxm61@psu.edu and Corry Rubber Corporation, 601 West Main Street, Corry, PA 16407 USA

[b] NIOSH, 626 Cochrans Mill Rd, Pittsburgh, PA 15236 USA; dcy6@cdc.gov.

[c] Penn State Erie, The Behrend College, School of Engineering, 5101 Jordan Road, Erie, PA 16563 USA; dhj1@psu.edu.

[d] Corry Rubber Corporation, 601 West Main Street, Corry, PA, 16407 USA; ebferro@corryrubber.com

[e] Kennametal, 442 Chalybeate Rd., Bedford, PA 15522 USA; chad.swope@kennametal.com.

Abstract

Among underground coal miners, hearing loss remains one of the most common occupational illnesses. In response to this problem, the National Institute for Occupational Safety and Health (NIOSH) Office of Mine Safety and Health Research (OMSHR) conducts research to reduce the noise emission of underground coal-mining equipment, an example of which is a roof bolting machine. Field studies show that, on average, drilling noise is the most significant contributor to a roof bolting machine operator's noise exposure. NIOSH OMSHR has determined that the drill steel and chuck are the dominant sources of drilling noise. NIOSH OMSHR, Corry Rubber Corporation, and Kennametal, Inc. have developed a bit isolator that breaks the steel-to-steel link between the drill bit and drill steel and a chuck isolator that breaks the mechanical connection between the drill steel and the chuck, thus reducing the noise radiated by the drill steel and chuck, and the noise exposure of the roof bolter operator. This paper documents the evolution of the bit isolator and chuck isolator including various alternative designs which may enhance performance. Laboratory testing confirms that production bit and chuck isolators reduce the A-weighted sound level generated during drilling by 3.7 to 6.6 dB. Finally, this paper summarizes results of a finite element analysis used to explore the key parameters of the drill bit isolator and chuck isolator to understand the impact these parameters have on noise.

[1]This is the third paper published in NCEJ on the special topic of Noise in Mines.

[2]The findings and conclusions in this report are those of the author(s) and do not necessarily represent the views of the National Institute for Occupational Safety and Health. Mention of any company of product does not imply endorsement by the National Institute for Occupational Safety and Health.

1 INTRODUCTION

Hearing loss prevention is one of the twenty-one Priority Research Areas listed in the NIOSH National Occupational Research Agenda[1]. Further, the Department of Labor Mine Safety and Health Administration (MSHA) collects noise exposure data that NIOSH OMSHR uses to help identify equipment whose operators are most likely to be overexposed to noise[2]. MSHA data collected from 2000 to 2005 show that seven types of machines compose the bulk of the equipment whose operators exceed 100% noise dose per the MSHA Permissible Exposure Level (PEL) (Table 1). Considering the operators of equipment used in underground coal mining, roof bolting machine (RBM) operators were the second-most likely to be overexposed to noise.

To develop effective noise controls for RBMs, it is important to determine the tasks and the corresponding sound levels associated with an RBM operator’s noise exposure. The objective was to reduce an RBM operator’s noise exposure to a time-weighted average (TWA) sound level of 90 dBA or less for an eight-hour shift. This corresponds to a noise dose of 100%, the maximum allowed per the MSHA PEL. NIOSH OMSHR collected noise dosimetry data to determine the sound levels and the noise doses associated with the tasks performed by an RBM operator. In addition, time-motion studies were performed to document the time spent conducting these tasks. Post-processing this data identified the tasks to which the operator devoted the most time, the noise dose accumulated during each task, and the tasks that are the primary contributors to the operator’s noise exposure. This information helped NIOSH OMSHR to determine where noise control development should be focused.

Tables 2 and 3 summarize data collected during a time-motion study of both operators of a dual-boom J.H. Fletcher roof bolting machine[3]. The operators were engaged in these tasks for at least 1% of their shift. The ‘other’ category of Tables 2 and 3 includes the time the operators spent riding the elevator or bolting alone, and times when their activity could not be documented. Table 2 shows that the operators spent a significant amount of time drilling and bolting simultaneously, roughly 3½ hours of the shift. Shown in Table 3, Operator 1 accumulated 52% PEL dose during this time, two-thirds of his daily noise exposure, 78% PEL dose. Operator 2 accumulated 68% PEL dose during this time, greater than half of his full-shift exposure, 127% PEL dose. Further analysis showed that the TWA sound levels for drilling exceeded those associated with bolting (Table 4).

With typical drilling times and proportionately short bolting times when installing resin-type roof bolts, the operators spent significantly more time drilling than bolting. These observations confirmed that for RBM operators, the drilling portion of the RBM duty cycle exposed them to the highest sound levels and it was the most significant contributor to their noise doses. Therefore, in order to efficiently reduce RBM operators’ noise exposures, noise controls must be developed that decrease the noise generated during drilling.

In percussive rock drilling, one notable source of noise generation is drill steel vibration[4,5]. There are three fundamental ways to reduce these vibrations, and the resulting noise: reduce the source of the vibration, attenuate the vibration using isolation or damping treatments, or attenuate the noise with barriers or absorbers. NIOSH sought to quantify the vibration levels of the components associated with drilling on the roof bolting machine. These included the drill head, slinger plate, drill guide, drill steel, and the drill media.

Figure 1 shows a slip ring assembly used to interface accelerometers on the drill steel with data acquisition equipment. Figure 2 shows a 5-second sample of the acceleration measured on a hexagonal drill steel when drilling into granite with a 35-mm-diameter bit using a rotation speed of 200 RPM and thrust of 9.4 kN. Granite was used as the drill media to represent a mine roof with a high compressive strength and because experience has shown that using granite helps to ensure test repeatability. The acceleration peaked at more than 500 g, confirming there is significant amount of drill steel vibration during drilling.

NIOSH used a 42-microphone Bruel and Kjaer beamforming array and the associated data acquisition system and analysis software to identify sources of drilling noise. A microphone was placed near the RBM operator’s head to measure operator ear sound levels. Once again, granite was used as the drill media for the aforementioned reasons. Figure 3 shows the beamforming results collected using a thrust of 9.4 kN and a rotation speed of 200 RPM. Light colors indicate areas of high noise radiation, while dark colors indicate areas of lower noise radiation. The results show one noise source centered on the drill steel and located roughly 100 to 200 mm (4 to 8 inches) below the drill steel-media interface and one noise source located just above the chuck. As the drill steel advances during drilling, the noise source near the chuck advances with the chuck, while the upper source remains just below the media.

Because the drill steel was shown to have high vibration levels and the beamforming images indicated that the drill steel and chuck are the sources of drilling noise, vibration isolation and damping are appropriate noise control methods. A 58 durometer (Shore D) jaw-type shaft coupling was used as a simple vibration isolator to test the premise that reducing the mechanical coupling between the drill steel and the chuck would reduce sound levels at the operator’s position (Fig. 4). Using the jaw-type coupling reduced the sound level at the operator’s position from a baseline of 100 dBA to 96 dBA when drilling with 9.4 kN of thrust, and from 104 dBA to 100 dBA when drilling with 22 kN of thrust. Figure 5 shows beamforming results with the inclusion of the jaw-type coupling for the same operating conditions as the baseline measurements. The figure shows the coupling reduced the contributions of both noise sources. Because prior measurements showed that the vibration levels on the drill steel were high, drilling noise was shown to come from the drill steel, and a simple vibration isolation device reduced the noise generated during drilling, NIOSH OMSHR considered vibration isolation to be a viable option to reduce drilling noise.

Most of the noise emitted during drilling is due to noise radiated by the drill steel and chuck in response to forces at the bit-rock interface. During drilling, the vibratory forces generated at the bit-rock interface are transmitted to the drill steel and to the chuck. The vibratory forces cause the drill steel and chuck to vibrate. Assuming linear viscous damping, the response of the structure is governed by

$$[M]\ddot{X}+[C]\dot{X}+[K]X=[F] \quad (1)$$

where [M], [C], and [K] are the mass matrix, damping matrix, and stiffness matrix of the structure; [F] is the vector of applied forces; and $\ddot{X}$, $\dot{X}$ and X are the acceleration, velocity, and displacement response of the structure. Using the Laplace transform, substituting $s = j\omega$, and rearranging Eqn. (1) to solve for X yields

$$[X]=\left[K+j\omega C-\omega^2 M\right]^{-1}[F] \quad (2)$$

where ω is the forcing frequency in units of rad/s and j denotes the $\sqrt{-1}$.

Assuming the damping is small enough to be ignored compared to the stiffness and the mass times the frequency squared, Eqn. (2) is reduced to

$$[X]=\left[K-\omega^2 M\right]^{-1}F. \quad (3)$$

For a fixed stiffness, Eqn. (3) shows that the response decreases with frequency squared once the frequency is well beyond the value where the $\omega^2 M$ term exceeds the stiffness, K. If the stiffness of the system is reduced, the frequency at which the $\omega^2 M$ term exceeds the stiffness term decreases. Thus, isolation is achieved by decreasing the stiffness of the system. The stiffness of the system can be decreased by adding compliance via an isolation device. This would decrease the response of the system to high frequency input forces.

For a vibrating object, the sound power radiated is given by

$$W=\langle\nu\rangle_{s,\tau}^{z} S\rho c\sigma \quad (5)$$

where W is the sound power radiated, $\langle\nu\rangle_{s,\tau}^{z}$ is the surface-averaged mean-squared vibration velocity, S is the surface area, and σ is the radiation efficiency[6]. Equation (5) shows that the sound power level radiated by a vibrating structure will be reduced if the surface-averaged mean-squared vibration velocity is reduced. The surface-averaged mean-squared vibration velocity is directly related to the displacement response of the system, so reducing the displacement response of the system will reduce the radiated noise. This can be accomplished with a properly designed vibration isolator.

Further development of a vibration isolation noise control device required the aid of a collaborating partner that is proficient in the design and production of vibration isolators. Therefore, NIOSH began working with Corry Rubber Corporation and Kennametal, Inc. on drill bit and chuck isolators.

2 DESIGN OVERVIEW

The first generation production drill bit isolator (BISO) and chuck isolator (CISO) designs are shown in Fig. 6. These designs evolved from several prototype designs that were evaluated for noise attenuation and durability. The isolators consist of three main components: the inner steel member, the outer steel member, and the elastomer. The elastomer is chemically bonded between the inner and outer steel members and the elastomer provides compliance (and therefore isolation) in multiple directions. Some of the earlier designs consisted of a bonded joint (elastomer bonded to the inner member) which was subsequently assembled into an outer member. These "pre-compressed, bonded joint designs" utilized a post-vulcanization (PV) bond between the outer surface of the elastomer and the inner surface of the outer steel member to react cutting forces. Advantages of pre-compressed bonded joint designs include improved elastomer durability (after assembly, the elastomer is in compression) and ease of manufacture because the mold has to accommodate only one metal and, therefore, one bond.

While these designs provided sufficient noise attenuation, they did not meet the load carrying requirements due to the relatively low bond strength and variability associated with PV bonds. The current production designs are fully bonded, which means the elastomer is bonded directly to the metal components during the molding operation. Fully bonded joints have superior bond strength compared to PV bonds. Based on lab testing, the production designs attenuate noise and meet all load requirements.

A typical cross section of the first generation production CISO design is shown in Fig. 7. The outer and inner members are machined out of 4130/4140 steel and heat treated to 35 HRC. Various elastomers were evaluated for noise attenuation as part of a design of experiments, but the production elastomer will more than likely be a 55 durometer (Shore A) natural rubber (NR) blend. The bonded length of 254 mm is consistent across all designs and it is necessary to safely react cutting forces through the elastomer section. An 11.4-mm-gap protects the elastomer from overload because the outer member will bottom out against the inner member at an axial load of roughly 45 kN. Any axial load above 45 kN will be reacted by the metal components instead of the elastomer. The design requirements for an isolator used to drill 35-mm-diameter holes are detailed in Fig. 8 and are summarized as follows:

1. Maximum torque: 410 N-m
2. Maximum axial load (thrust load): 35 to 45 kN
3. Isolator metals will bottom out at 11.4 mm deflection or approximately 45 kN thrust load
4. Preliminary life requirement: 2 weeks to 1 month of continuous operation
5. Estimated static axial stiffness (for noise attenuation): 2,600 to 5,200 kN/m
6. Estimated torsional static stiffness (for noise attenuation): 6.8 to 20.3 N-m/deg
7. Cocking and radial stiffness should be sufficiently high to avoid excessive elastomer strain

The stiffness requirements were based on sound level measurements using prototype isolators. The sound level at the operator's location was measured during "normal" drilling and also with several prototype isolator parts with varying stiffness. The production designs meet the requirements listed above. Extensive lab testing and analysis was performed on the production design to verify these requirements. The drill bit isolators do not significantly change the ordinary operation of the roof bolting machine. Therefore, addition of the isolators has no impact on the time or effort required to install roof bolts.

3 ELASTOMER COMPOUND EVALUATION

Fine powders are generally added to rubber to change the properties of the material. Examples of the properties that can be altered by these fine powders are tensile strength, hardness, shear modulus, ultimate elongation, and compression set resistance. Carbon black is the most widely used fine powder. With elastomers that crystallize upon extension, such as natural rubber, it is not necessary to add carbon black to achieve high tensile strengths. However, most elastomers do not crystallize upon extension and, therefore, require some amount of carbon black to reach their maximum tensile strength. Even though natural rubber crystallizes upon extension, which provides good tensile strength, natural rubber is a soft material without reinforcement, typically exhibiting a Shore A hardness of approximately 30 to 35. The applications for rubber with such a low hardness are limited. But, carbon black can be added to raise the hardness and shear modulus while preserving good tensile strength. Increasing levels of carbon black generally results in an increase in tensile strength until a maximum tensile strength is reached. Once this maximum tensile strength is reached, the tensile strength tends to drop off as more carbon black is added. The carbon black essentially acts as a reinforcing agent up to the point where the tensile strength is at a maximum (for NR compounds, around 50 durometer Shore A). Beyond that level, the carbon black becomes more of a filler than a reinforcing agent, so tensile strength tends to drop off at higher loadings. Finally, as the level of carbon black in a compound is increased, the damping of that compound, the ability to convert energy into heat, increases. Depending on the properties required by the final product, the level and type of carbon black used can be selected to tailor the properties of the compound to those required by the application.

In an effort to explore how material impacts isolator performance, several isolators were made with various elastomer compounds (Fig. 9). These elastomers were selected to provide a broad range of dynamic and static properties for sound level evaluation while still satisfying the requirements outlined above. A description of each elastomer compound evaluated is shown in Table 5. The natural rubber compounds have a range of tensile modulus varying from 1.6 MPa (45 durometer Shore A compound) to 4.1 MPa (68 durometer Shore A compound). The butyl compound was developed to provide approximately the same static stiffness as the 45 durometer Shore A natural rubber, but with four times as much damping. Furthermore, the 58 durometer Shore A and 45 durometer Shore A natural rubber compounds have nearly the same damping but different stiffness. The idea here is to explore the effects damping and stiffness have on noise attenuation. The compounds selected provide an adequate range for these properties.

4 STATIC AND DYNAMIC STIFFNESS TESTING

Isolators bonded with the elastomers detailed in Table 5 were tested in the lab in the torsional and axial directions. The test machines used for this testing are shown in Figs 10 and 11. The purpose of this testing was to verify that the stiffness and load requirements were met. A summary of the testing and results follows.

1. Axial static stiffness test – record load versus deflection curve up to 7.6 mm deflection. See Fig. 12.
2. Axial static stiffness test – record load versus deflection curve up to18 kN.
3. Dynamic stiffness at 5 +/− 0.5 mm – perform frequency sweep from 1 Hz to 30 Hz in 3 Hz increments. Record dynamic stiffness, K', damping stiffness, K", and loss factor (tan del). See Fig. 13 for dynamic stiffness, K', versus frequency.
4. Torsion test - load to approximately 410 N-m (the design torque requirement) and record torque versus angular deflection curve. See Fig. 14.
5. Torsion test to failure to determine failure torque and angular displacement.

5 DISCUSSION OF EXPERIMENTAL STATIC AND DYNAMIC STIFFNESS RESULTS

The static and dynamic axial stiffness and the static torsional stiffness for the tested isolators are summarized in Table 6. The calculated results for the radial and cocking stiffness are included for reference only. Based on lab testing, the following observations can be made:

1. The measured stiffness (both axial and torsional) is consistent with the durometers specified in Table 5 for each compound. In other words, the 68 durometer NR has the highest torsional and axial stiffness followed by the 58 durometer and then the 45 durometer compounds. The dynamic axial stiffness of the 68 durometer NR compound is nearly twice that of the 45 durometer NR compound due to increased damping and modulus. Therefore, these three durometers provide a broad range of stiffness for noise evaluation.
2. The 50 durometer heavily damped butyl is highly frequency sensitive (see Fig. 13). While the 50 durometer butyl isolator's static stiffness is nearly the same as the 45 durometer natural rubber isolator, its dynamic stiffness at 30 Hz is more than twice that of the 45 durometer natural rubber isolator. This frequency sensitive behavior is typical of heavily damped elastomer compounds. The noise and vibration benefits from high damping may be offset by the higher dynamic stiffness at higher frequencies.
3. All of the measured axial and torsional stiffness values met the design requirements and were verified with FEA and hand calculations. Based on lab results and analysis, the design curve in Fig. 15 was constructed. This curve shows the locus of all possible torsional and axial stiffness for the production isolator configuration as a function of durometer. The expected stiffness tolerance for an isolator made from a 55 durometer natural rubber compound (the production elastomer) is shown as a shaded box in the figure. Note the broad range of axial and torsional stiffness possibilities by just changing the compound durometer.
4. The axial and torsional load requirements of 45 kN and 410 N-m were safely met by all isolators. The metal components showed no evidence of yielding and the elastomer showed no evidence of tensile failure or bond failure at these loads. Additionally, two isolators were loaded to failure on the torsion machine with

failure torques of 730 N-m and 760 N-m, which are nearly twice the torque requirement.

6 TEST SETUP AND RESULTS FOR SOUND LEVEL MEASUREMENTS

A computer-controlled drilling apparatus (see Fig. 16) was used to test the bit and chuck isolators made with the natural rubber compounds. Problems with the vacuum system on the test apparatus prevented testing of the isolators made with butyl rubber. An optical tachometer was used to check the rotational speed for each test. A Bruel & Kjaer Type 4188 microphone was positioned roughly one meter from the drill steel at a height of about 1.5 meters.

For all testing, 35-mm-diameter drill bits were used with hexagonal drill steels. A 1.4-meter-long drill steel was used for baseline measurements. When the bit and chuck isolators were tested, shorter drill steels were used to maintain a total length of 1.4 meters. Measurements with either a bit isolator or a chuck isolator were performed using a 1.0-meter-long drill steel while measurements with both a bit isolator and a chuck isolator were completed with a 0.7-meter-long drill steel.

All tests were performed with a rotational speed of 270 RPM, a penetration rate of 28 mm/sec, and a maximum thrust of 22 kN. An LMS Pimento portable data acquisition system was used to record the sound pressure using 24-bit resolution at 20,000 samples/second. The microphone data were post-processed to calculate the A-weighted 1/3-octave-band sound levels according to ANSI standards[7]. While time-weighted average (TWA) sound levels, which are affected by the noise dosimetry parameters (threshold level, criterion level, exchange rate, etc.), were used when collecting the field data, the equivalent continuous sound level was calculated for the laboratory tests. For a fixed drilling time, a change in the equivalent continuous sound level would yield a corresponding change in the TWA sound level. Table 7 summarizes the various test configurations and results for the sound level measurements. A detailed discussion of each test follows.

Prior to performing measurements while drilling, the sound pressure was measured with only the hydraulic and vacuum systems operating. Figure 17 shows the A-weighted sound levels in 1/3-octave bands with the hydraulic and vacuum systems operating without drilling and while drilling with a 1.4-meter-long hex drill steel. The figure clearly shows that noise from the hydraulics and vacuum are insignificant compared to drilling noise. The levels in the 400 Hz through 10 kHz 1/3-octave bands increase by 10 dB or more with drilling. In addition, the levels at and below 315 Hz do not change much which suggests the noise at these frequencies is due to the hydraulics and vacuum systems instead of drilling. The highest in-band levels are in the 2500, 3150, and 4000 Hz 1/3-octave bands. The remaining figures will focus on the levels above 250 Hz because drilling noise does not have significant low frequency content.

Figure 18 shows the results for the tests with bit isolators compared to the baseline. The figure shows that each of the bit isolators significantly reduced drilling noise above 1600 Hz. The 45 durometer bit isolator achieved the highest reductions, while the 68 durometer bit isolator yielded the least reductions. The 45, 58, and 68 durometer bit isolators reduced the overall A-weighted sound level by 6.6, 5.9, and 3.9 dB, respectively. Since the stiffness of a rubber component decreases as durometer decreases, the data suggest that decreasing the stiffness of the bit isolator could further reduce the sound level. However, reducing the durometer can have a negative impact on the life of the part due to increased strain levels.

Due to time constraints, just one test was conducted with an isolator only at the chuck location and without a bit isolator. Figure 19 shows the resulting spectra for the baseline compared to the test with a 58 durometer chuck isolator. The figure shows that the chuck isolator substantially reduced the levels above 1600 Hz, and it reduced the overall A-weighted sound level by 3.7 dB. Based on this encouraging result, future testing will be expanded to include multiple durometer isolators at the chuck location.

The data were analyzed to determine the benefit of using both a bit isolator and a chuck isolator compared to only using a bit isolator. Figure 20 shows the resulting 1/3-octave band spectra for drilling with a 58 durometer bit isolator and with both a 58 durometer bit isolator and chuck isolator. Combining a chuck isolator with a bit isolator resulted in a slight additional reduction of the in-band levels for some frequencies. However, the changes are so small they could be due to test-to-test variation.

Combinations of bit and chuck isolators of the same durometer were tested to explore their effect on the noise generated by drilling. Figure 21 shows the results for these combinations along with the results for baseline conditions. The figure shows that the levels with the 58 durometer isolators are lower than those with either the 45 or 68 durometer isolators. This is somewhat surprising since isolation usually improves as stiffness is reduced. However, the figure shows the combination of the least stiff isolators – the 45 durometer parts – resulted in higher levels. This could be a result of the lower stiffness chuck isolator allowing the drill steel to drill an out-of-round hole. This would tend to cause the sides of the drill steel to rub against the insides of the hole which would increase noise. To fully examine this phenomenon, future testing should explore combining a low stiffness bit isolator and chuck isolators with a wide range of stiffness.

Figure 22 shows the results for the best three tests with bit and/or chuck isolators compared to the baseline results. The figure shows that using a 45 durometer bit isolator resulted in the greatest reductions. However, Fig. 20 shows each of these tests resulted in substantial sound level reductions in the 1/3-octave bands at and above 1600 Hz. While all the tested isolators reduced the A-weighted sound level whether used singly or in combination, the 45 durometer natural rubber bit isolator achieved the highest reduction, 6.6 dB, while the 58 durometer natural rubber bit isolator yielded a reduction of 5.9 dB.

7 SECOND GENERATION PRODUCTION DESIGN (ISOLATOR REFINEMENT)

The first generation production designs detailed above and shown in Figs 6 and 7 met the design requirements for noise reduction, stiffness, and load-carrying ability. These designs were subsequently evaluated in the field at various mines throughout the United States. Based on feedback from the field, certain design improvements were incorporated into the outer metal component resulting in a second generation production design. The second generation design is shown in Figs 23 and 24. The bonded area (elastomer) and inner member did not change, but the outer member was changed to a two-piece design. The two-piece design incorporates an end cap welded to the outer member after the elastomer is bonded to the outer member and the isolator is removed from the mold. Because both ends of the isolator have male connections, the isolator can be positioned at any point along the length of a drill rod. These features give the second generation design the following advantages:

1. The isolator becomes a universal design meaning the same part can be used at both the drill bit and chuck locations. This effectively eliminates an entire design and two complex metal components. Because a single design can be used, the production volume is expected to increase which would reduce the cost of the isolator.
2. The drill bit seat is no longer an integral part of the isolator. Consequently, if the bit seat wears, a simple insert is replaced versus an entire isolator.
3. A complex cleaning operation that was necessary to remove elastomer from inner diameter of isolator to prevent clogging (cutting off of vacuum) is no longer required.

A small production quantity of the second generation design has been completed. These parts are scheduled to undergo lab testing and field evaluation as part of the product approval process.

If necessary, other methods exist to improve isolator load capacity and durability. Two of these methods are shown in Fig. 25. Figure 25 shows two options where the metals are designed to limit isolator travel to protect the elastomer from overload. Under normal operating conditions, the cutting forces would be reacted by the elastomer, so isolation would be achieved. This feature is similar to the axial clearance feature present in the current designs to protect isolators from axial overload. Overload protection in both directions might allow the length of the isolator to be shortened because the maximum loads on the elastomer are now limited.

Figure 25 shows yet another way to improve isolator durability. With option B, the metal components would be manufactured in such a way that the inner diameter of the outer member and outer diameter of the inner member result in an elliptical elastomer section. With this design, at small torsional displacements the elastomer would be loaded mostly in shear, which would provide a low spring rate for good isolation. However, at higher torsional displacements, the elastomer would be loaded in compression, which would increase the isolator stiffness and the torsional capacity.

8 DEVELOPMENT OF ALTERNATIVE CHUCK ISOLATORS

All of the CISO and BISO isolators detailed above are designed to pass through the hole during drilling without contacting the sides of the hole. This constrains the outer diameter of the isolator to a maximum value of approximately 35 mm. Because cutting forces are reacted entirely through shear of the elastomer and bond, the isolators must have sufficient length (i.e. 125 mm) to endure the applied loads. The small diameter, long length, and large length-to-diameter ratio could negatively impact the design in the following ways: high cocking and radial stiffness, high stress in the metal components, and potential durability issues with the elastomer due to high strain resulting from thin rubber wall. The initial approach was to use the same or similar designs for both the BISO and the CISO, which ultimately led to the development of the dual-purpose second generation isolator (QC-20377) shown in Fig. 24. Although using a universal design offers cost advantages, this approach does not take advantage of the increased space available at the chuck location. Consequently, a parallel path was undertaken to investigate various alternative chuck isolator designs. These alternate chuck isolators are expected to be used in conjunction with the standard BISO as shown in Fig. 26.

8.1 Prototype Alternative Chuck Isolators

Several alternative chuck isolator designs were optimized within a practical space envelope of 250 mm OD by 55 mm height. Two of these designs were prototyped and lab tested. The "EST" chuck isolator shown in Fig. 27 utilizes standard 35-mm-diameter shear mounts (CRC P/N EST14N). The number of EST14N mounts can be varied along two bolt circle diameters to produce a broad range of stiffness properties. Several configurations are shown in Fig. 28. The stiffness values for each configuration are listed in Table 8. These stiffness values are based on measured lab results for a single EST14N shear mount made from 55 durometer natural rubber. Similar to the production isolators above, the EST14N mount can be made from 30 to 90 durometer rubber. This would greatly expand the possible stiffness range of the CISO (i.e. values shown in Table 8 would be about 3X less stiff at 30 durometer and 3X more stiff at 90 durometer). Furthermore, the EST chuck isolator can incorporate a ring inside the outer member to restrict motion and to increase stiffness in the radial direction. The sound level results from Sec. 6 suggest there is an optimal stiffness for the chuck isolator. The EST coupling will be of great value to help identify this stiffness because a wide range of stiffness values can be explored easily by changing the configuration or mount durometer.

Another alternative chuck isolator that was designed and prototyped is shown in Fig. 29. The "pancake" chuck isolator utilizes molded disks as shown in Fig. 30. The size, durometer, arrangement (i.e. disks in parallel or series), and amount of pre-compression can greatly alter the stiffness of the coupling. The stiffness of this coupling is higher than the EST chuck isolator and more similar to the stiffness of the production isolators. The cocking stiffness, however, can be considerably lower when thin, low stiffness disks are used in series. Together, this pancake chuck isolator and the EST chuck isolator cover a broad range of stiffness in all directions. Again, the various configurations of the chuck isolator can be used in conjunction with a production drill bit isolator to identify the best stiffness combination.

8.2 Possible Alternative Production Chuck Isolator Designs

The intent is to perform sound level measurements using the two prototype chuck isolators described above with and without the production QC-20377 isolator at the bit location. To verify durability of these designs, it is expected that these designs will also be tested in the field. Once the stiffness attributes are properly defined, a production version will be designed. Four possible configurations are shown in Fig. 31. Each of these configurations offers a unique advantage as described in the figure. Option A is similar to the prototype pancake chuck isolator except the elastomer is bonded to a metal insert. Bonded designs produce consistent stiffness over long periods of time. The bonded metal insert is pre-compressed into two metal housings with attachment features on the ends. This design would have a higher cocking and radial stiffness but have tremendous axial and torsion capacity and would be quite durable. Option B is a cost-effective, fully bonded isolator. This design has stiffness similar to Option A and the prototype pancake isolator, but is not pre-compressed. Because the elastomer is not pre-compressed, this design may not have the durability of the others, but it would still be more durable than the production chuck isolators because the thrust load is carried in compression versus shear for the production isolators. Finally, Options C and D are conical shaped. These designs offer much lower cocking and axial stiffness and are pre-compressed for durability.

In summary, a great deal of effort has been spent investigating various alternative chuck isolator designs. Taking advantage of increased space at the chuck location results in unique alternative chuck isolators, which offer the following potential advantages:

1. Increased durability. Torque is reacted at a much larger diameter so stress is considerably less. Axial load is reacted in compression (versus shear) which is a more favorable loading for elastomer. Stresses in the metal components are significantly lower. Finally, these elastomer in these designs can be pre-compressed for improved elastomer fatigue life.

2. Tunability. Modular designs allow for a wide range of stiffness properties. Also, pre-compression can be adjusted to fine-tune stiffness.

3. Replacement cost. Due to the modular nature of these designs, wear items, such as the bonded joint, can simply be replaced.

4. Lower stiffness. Stiffness can be significantly lower for the alternative chuck isolators. Lower stiffness may result in better noise reduction.

5. Possible improvement in drill rod life. The cocking stiffness can be sufficiently low enough to allow the chuck isolator to act like a “spherical bearing” to decrease side loads on the drill rod. For example, from Table 8, the cocking stiffness of the EST coupling can be as low as 28 N-m/deg. This is 1000X lower than the cocking stiffness of a 1.2 m length of drill rod. Since the chuck isolator acts as a spring in series with the drill rod, any misalignment will result in a deflection of the isolator.

9 FEA SIMULATION

Finite element (FE) analysis was used to explore the key parameters of the bit isolator (BISO) and chuck isolator (CISO) designs. In the FE model, the BISO and the CISO are treated as simple longitudinal and torsional springs. In addition, longitudinal springs are used to connect the drill bit tip to the drilling media, which is expected to be rock. The simulation software used for this study was ANSYS version 12.1.

Figure 32 shows the FE model used for the analysis. The drill rod has a hexagonal cross section and it is modeled with 3D shell finite elements. The drill bit body is also modeled with 3D shell finite elements. At the end of each hexagonal body, multi-point constraints (MPCs) are used to connect the hex cross section to the isolator springs which are placed along the centerline of the drill rod assembly. MPCs define geometric relationships that must be met by the displacements of selected nodes of the structure. In this study, the MPCs connect the motion (translation and rotation) from the ends of the longitudinal and torsional springs to the ends of the hex-shaped drill rod and drill bit bodies. To represent the stiffness of the rock, longitudinal springs were used to connect the tip of the bit to ground. The axial and radial spring rates for these connections were 175.1 MN/m and 2,057 MN/m, respectively. These values were used to represent a rigid connection. The applied load can be tangential (FY) or axial (FZ), and it is placed off-center on the drill bit tip, representing the drill bit cutting edge interaction with the drilling media (rock).

Any preload of the elastomer isolator components was ignored for this study. It was also assumed that the stiffness and damping of the elastomer do not change with frequency to simplify these analyses. The weight (gravity load) of the drill string was ignored as well, because this study focused on the dynamic loading that occurs during the drilling process.

Prior to solving for the models dynamic response, a mesh refinement study was performed using modal analysis. The first ten natural frequencies were found using ANSYS. The mesh was refined in successive steps until minimal variation was observed in the first ten natural frequencies. Then, forced vibration, or “harmonic” analysis, was used to simulate the drilling operation and to predict drill rod vibrations.

Harmonic analysis is a class of dynamic analysis simulations where the goal is to find a sustained cyclical response (a harmonic response) in a structural system, caused by a sustained cyclical load. A unit force with a flat frequency spectrum over the frequency range of 446 to 3550 Hz was applied to the drill bit tip. This frequency range was selected because prior research has shown the 500 Hz through 3150 Hz 1/3-octave bands dominate the noise radiated by the drill rod. The unit force was applied tangential to the circumference of the drill bit tip. This force orientation was selected to excite bending modes in the drill rod. It is these bending modes that probably radiate most of the drilling noise.

The FE program utilities for vector and matrix data operations were quite valuable in this study. From the harmonic analysis, the displacement response was calculated at 3104 frequency intervals from 446 to 3550 Hz in 1-Hz increments. Then, the drill rod displacements were collected at ten locations along the length of the drill steel. At each location, the displacements at the center of each hex face were stored for a total of 60 points at each frequency interval. To separate the radial, tangential, and axial displacements, the displacements were transformed into a polar coordinate system. Because the noise radiated by a structure is related to the vibration normal to its surface, the radial displacement was of primary concern.

9.1 Estimation of Sound Power Level Radiated by the Drill Rod

The FE results were used to estimate the sound power level radiated by the drill rod. For a vibrating object, the sound power level radiated can be estimated by

$$L_W=10log_{10}\langle\nu\rangle_{s,t}^2+10log_{10}S+10log_{10}\sigma+146\left(dB \quad re \quad 1^{-12}watts\right) \quad (7)$$

where L_W is the sound power level, $\langle\nu\rangle_{s,\tau}^z$ is the surface-averaged mean-squared velocity, S is the surface area, and σ is the radiation efficiency[7]. For each the displacement results from the FE model, the ANSYS vector and matrix data utilities were used to calculate the velocity response at each point by

$$\nu=2\pi fr \quad (8)$$

where r is the magnitude of the radial displacement as a function of frequency and f is the excitation frequency in Hz. The surface-averaged mean-squared velocity response of the drill rod was then calculated by squaring and averaging the calculated velocities along the drill rod.

The radiation efficiency of the drill rod was assumed to be unity in the frequency range analyzed. The actual radiation efficiency would not be unity, but for comparison purposes and trend analysis with the FEA model, this is an acceptable approximation. Equation (7) was evaluated in the FEA model to predict the sound power level radiated by the drill rod for each analysis case. Within the evaluation process, A-weighting was applied to the estimated sound power levels because regulatory standards in mining define the allowable worker noise exposure in terms of the A-weighted sound level[8]. For each analysis case, the A-weighted 1/3-octave-band sound power level spectrum was computed by summing the narrowband sound power from the lower cutoff frequency to the upper cutoff frequency for each 1/3-octave band from 500 Hz through 3150 Hz. Finally, the overall A-weighted sound power level from 446 to 3550 Hz was calculated by summing the A-weighted narrowband sound power levels.

Numerous analyses were conducted with a wide variety of BISO and CISO stiffness values. Table 9 lists the stiffness values used for the BISO and CISO and the FEA model prediction of sound power levels for 17 analysis cases. The axial spring is aligned with the longitudinal axis of the drill rod. The torsional spring corresponds to rotation about the longitudinal axis of the drill rod, while the cocking spring resists rotations about the radial direction. The rigid case is representative of a drill rod without a BISO or CISO. Simulation cases 1 through 8 correspond to the current production design (see Fig. 6 or Fig. 23) where the BISO and CISO stiffness conditions were varied from flexible (30 durometer) to stiff (90 durometer). The medium condition corresponds to measured stiffness values with the current production elastomer (55 durometer). Simulation cases 9 through 16 represent a production BISO used in conjunction with an alternative chuck design. This arrangement (shown in Fig. 26) captures how a lower radial and cocking stiffness might impact results.

Table 10 shows a comparison of the experimental and FEA simulation results and supports the validity and value of the FEA model for trend analysis of the effects of the BISO and

CISO on the sound power level radiated by the drill steel. Several comparison cases between the experimental measurements and the simulation model were selected which exhibited similar conditions. While the estimates of the overall sound power level computed using the FE model cannot be compared with the overall sound power level of each case, the changes in the estimated sound power level predicted with the model can be compared to the changes observed in the laboratory testing when isolation was added to the system.

The sound power levels estimated for the FE model analyses were compared to reveal trends. Table 9 shows that Cases 3, 4, 5, 13, and 14 yield sound power levels close to that of the baseline case, Case 0. For each of these scenarios, the BISO is either rigid or stiff. Cases 4, 5, and 13, which use either medium or soft CISOs, show an insignificant reduction in the sound power level on the order of 0.1 dB. Cases 1, 2, 6, 7, 8, 9, 10, 11, 12, 15, and 16 reduce the A-weighted sound power level by approximately 10 dB. For each of these cases, the BISO is either soft or medium. The best reduction is observed for Case 2 with a medium BISO. Clearly, the results indicate the BISO is the critical component in terms of noise radiated by the drill rod. The CISO has little effect on the estimated sound power level.

9.2 Results for Sound Power Level

Figure 33 shows the FE prediction of sound power level spectra for the 500 through 3150 Hz 1/3-octave bands for Cases 0, 1, 2, 6, and 7. For the baseline case, Case 0, the sound power level spectrum is dominated by the 1/3-octave bands above 1250 Hz and it exhibits a dip at 1250 Hz. This dip shifts to the 800 Hz 1/3-octave band for Case 1 and to the 1000 Hz 1/3-octave band for Case 2. The spectra show that decreasing the stiffness of the CISO (Case 1 to Case 6 and Case 2 to Case 7) affects the levels in the 1/3-octave bands even though it does not significantly change the overall sound power level in the 500 Hz through 3150 Hz 1/3-octave bands. As the BISO and CISO spring rates change, the modes of the drill rod are affected due to the change in boundary conditions. In addition, the force transmission from the bit to the drill rod is affected by the BISO spring rate. Although the figure shows that switching from a rigid CISO to a flexible CISO adversely affects the higher frequency 1/3-octave bands, it is important to keep in mind that some of the drilling noise radiated with an actual roof bolting machine comes from the machine’s chuck. Because the model here does not include the chuck, it would be incorrect to conclude that decreasing the stiffness at the chuck would increase drilling noise.

10 CONCLUSIONS

The current designs of production bit and chuck isolators evolved from relatively simple isolation devices that were only suitable for laboratory testing. The first generation production designs were verified to meet design targets for spring rate, torque and load capacity, and sound level reduction. Testing with an automated drilling apparatus proved that bit and chuck isolators with natural rubber elastomers reduced the sound level near the drill steel. While all the tested isolators reduced the A-weighted sound level whether used singly or in combination, the 45 durometer natural rubber bit isolator achieved the highest reduction, 6.6 dB, while the 58 durometer natural rubber bit isolator yielded a reduction of 5.9 dB. Measurements with a combination of a bit isolator and chuck isolator revealed that the sound level could increase compared to isolator-only values if the stiffness of the chuck isolator is low. This suggests there is an optimal stiffness for the chuck isolator.

Based on field testing, a new and improved isolator (QC-20377) was designed and manufactured. The new isolator can be used at both drill bit and chuck locations so the need for two separate isolators is eliminated. Field testing of QC-20377 is in progress. Plans are in place to perform additional lab testing to identify optimal elastomer for the production QC-20377 isolator. Testing will also include evaluation of the various alternative chuck designs that were prototyped. These chuck designs offer flexibility in terms of fine tuning stiffness. Once the optimal chuck design has been determined, the stiffness properties will be designed into a production version.

FEA simulation of the drill string assembly has been identified as a useful tool in evaluation of BISO and CISO designs and combinations. Further, the simulation model can be used for cases with different drill rod lengths, providing insight into how the drill rod length affects the required isolator stiffness. The model will be used to determine if there is an optimum bit isolator and chuck isolator design combination.

In past studies, the chuck has been shown to be a significant radiator of noise[9]. For simplicity, the chuck was not modeled for this FE analysis. In real-life operating conditions, vibrations are transmitted down the drill steel and into the chuck. The chuck can then be set into vibration causing it to radiate noise. In order to better estimate the effect of CISO spring rates, the FE model would benefit by including a model of the chuck.

If necessary, improvement in the precision of the predicted sound power level may be achieved by determining the radiation efficiency of the drill rod and roof bolting machine chuck through experimental means using shakers to excite vibrations in each and microphones to measure the resulting noise. This effort may be unnecessary if it is adequate to use the FEA model to simply evaluate trends in response as opposed to predicting the precise levels of sound power.

11 REFERENCES

1. 1996. National Institute for Occupational Safety and Health, National Occupational Agenda, Department of Health and Human Services Publication No. 96-115
2. Title 30 CFR Part 62, 2000–2005, U.S. Department of Labor, Mine Safety and Health Administration, Information Resource Center
3. Peterson, Jeffrey Shawn; Alcorn, Lynn. Results of noise measurements from underground testing of a roof bolting machine duty cycle. NoiseCon07. 2007
4. Hawkes I, Burks JA. Investigation of Noise and Vibration in Percussive Drill Rods. Int. J. Rock, Mech, Min. Sci. & Geomech. 1979; 16:363–376.
5. Carlvik I. The Generation of Bending Vibrations in Drill Rods. Int. J. Rock, Mech, Min. Sci. & Geomech. 1981; 18:167–172.
6. Bies, DA.; Hansen, CH. Engineering Noise Control Theory and Practice. Third. Spon Press; New York, New York: 2003.
7. Octave-Band and Fractional-Octave-Band Analog and Digital Filters. 2009 ANSI/ASA S1.11-2004.
8. Department of Labor, Mine Safety and Health Administration. Health Standards for Occupational Noise Exposure: Final Rule. 1999 30 CFR Part 62. Federal Register.

9. Yantek DS, Peterson JS, Smith AK. Application of a microphone phased array to identify noise sources on a roof bolting machine. NoiseCon07. 2007

Author Manuscript
Author Manuscript
Author Manuscript

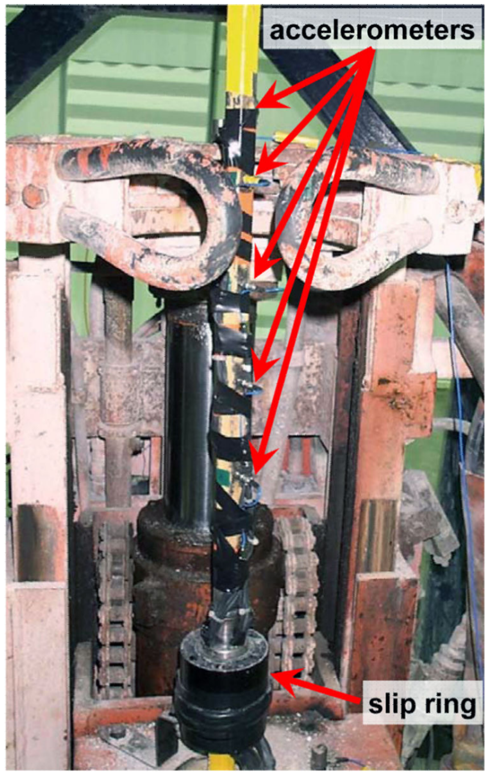

Fig. 1.
Drill steel accelerometers and slipring assembly.

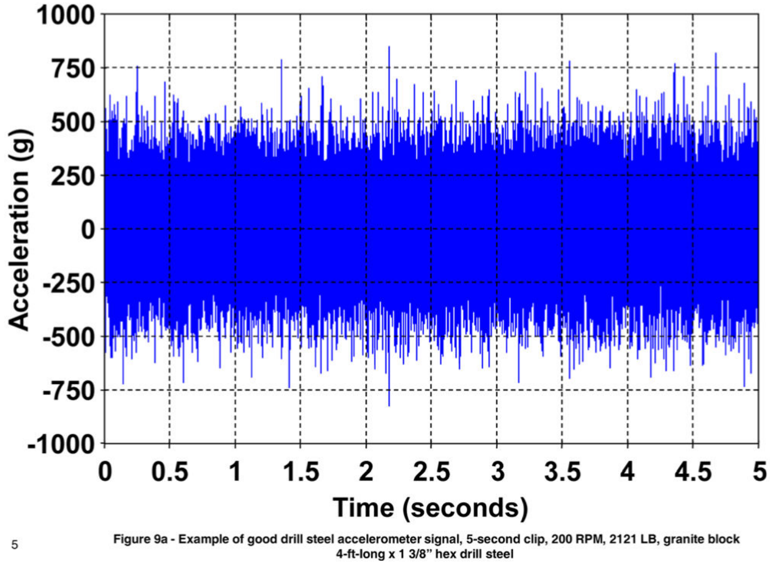

Fig. 2.
Typical drill steel acceleration, hexagonal drill steel, 35-mm-diameter bit, granite drill media.

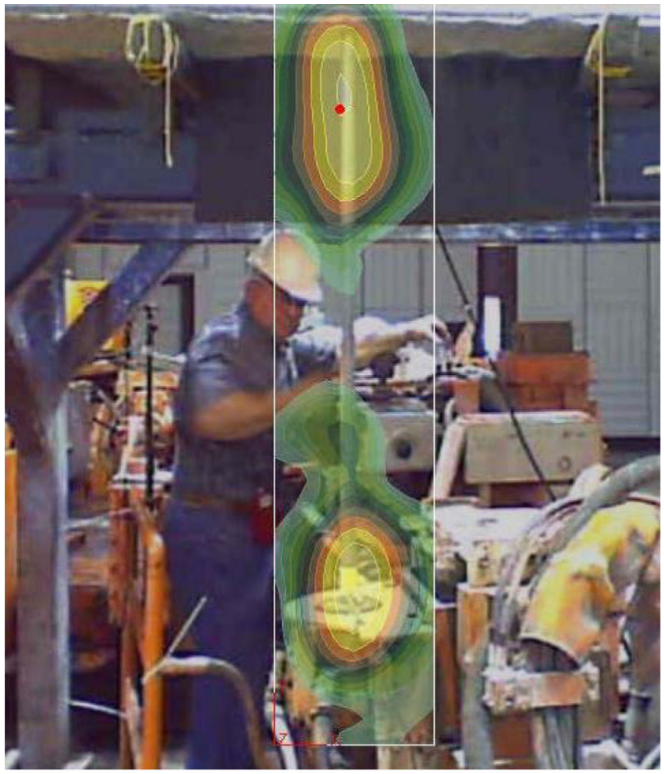

Fig. 3.
Beamforming image for baseline drilling, 100 dBA at the operators' position.

Fig. 4.
Jaw-type coupling with 58 Shore D urethane spider.

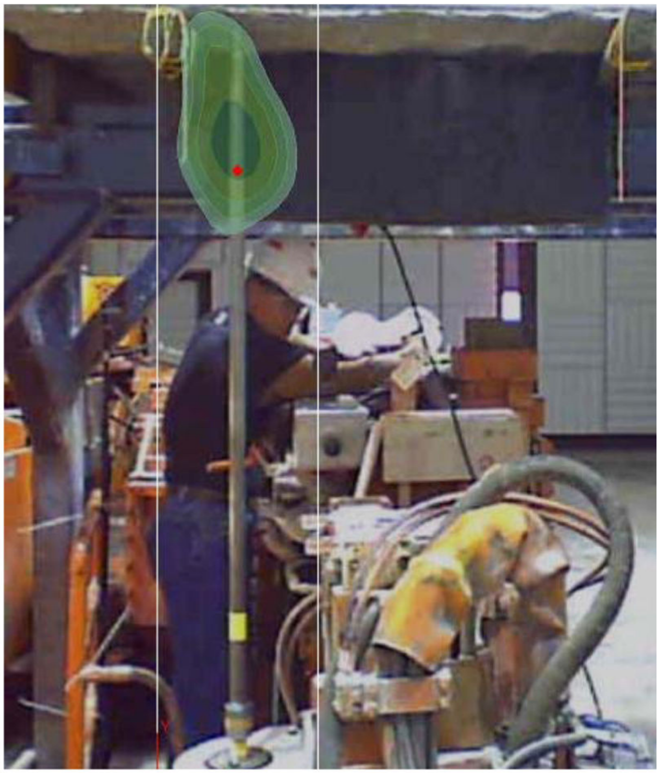

Fig. 5.

Beamforming image for drilling with the jaw-type coupling, 96 dBA at the operators' position.

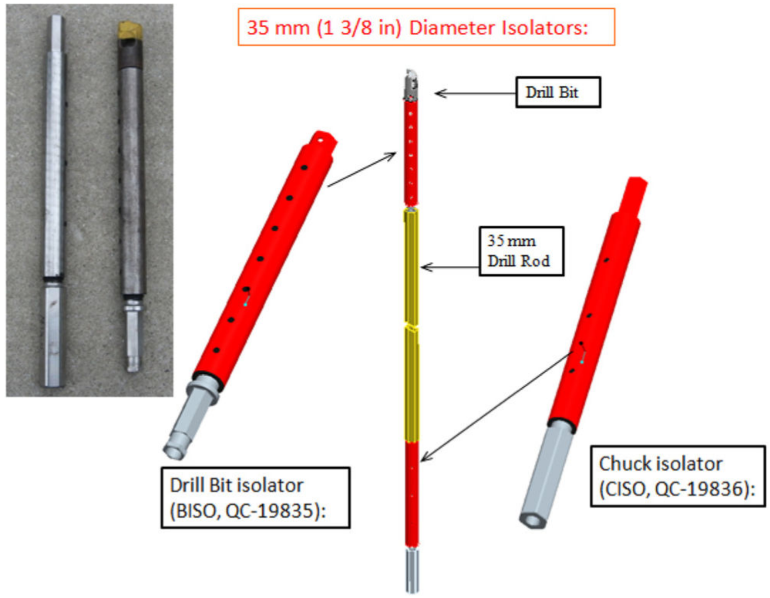

Fig. 6.
First generation production designs of isolators for use with 35-mm-diameter drill bits.

Author Manuscript
Author Manuscript
Author Manuscript

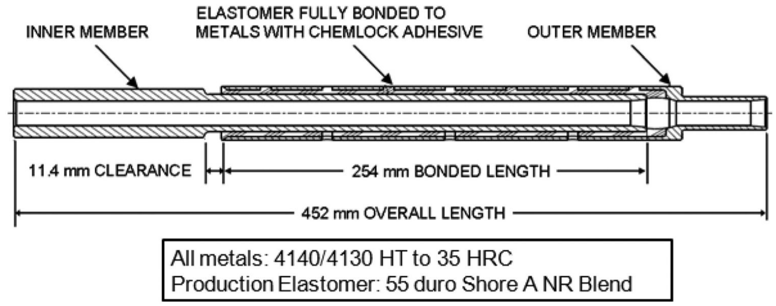

Fig. 7.
Cross-section of first generation production design chuck isolator.

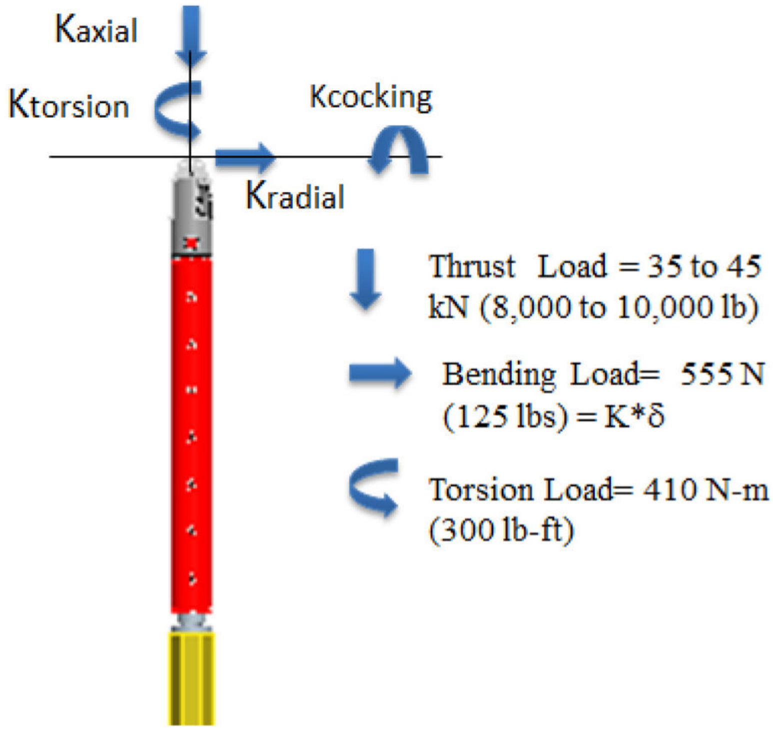

Fig. 8.
Design requirements for load and corresponding stiffness directions.

Fig. 9.
Isolators bonded with elastomers from Table 5.

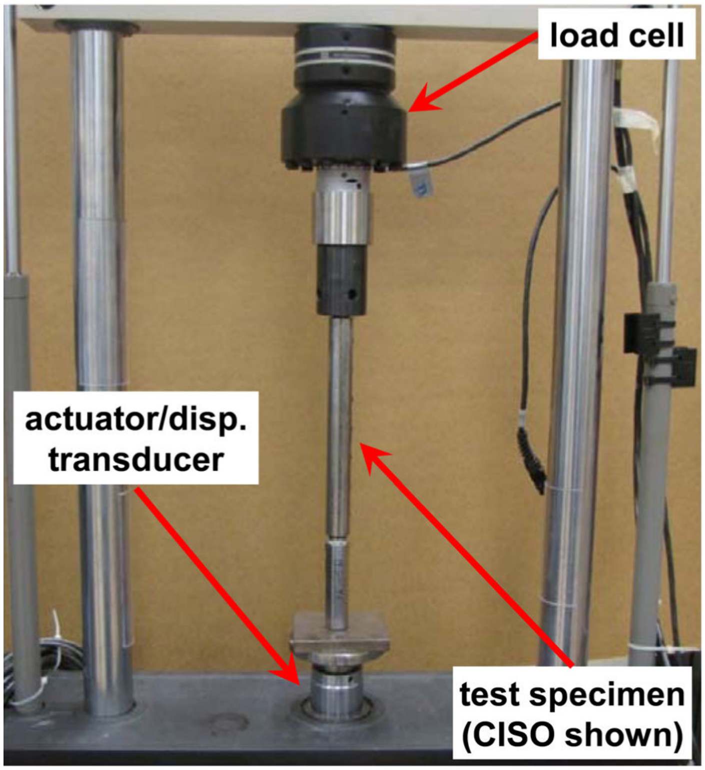

Fig. 10.
MTS810 test system used to measure axial load capacity and static and dynamic stiffness.

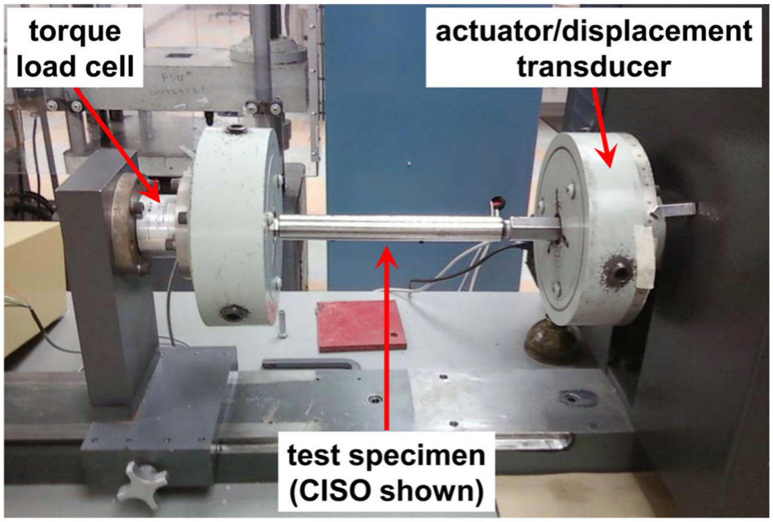

Fig. 11.
Apparatus used for testing torsional load capacity and static torsion stiffness.

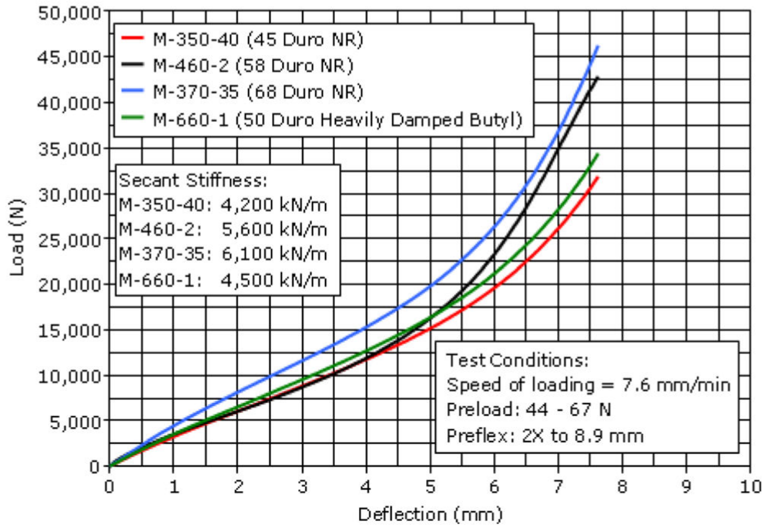

Fig. 12.

Axial test, static load-deflection curves.

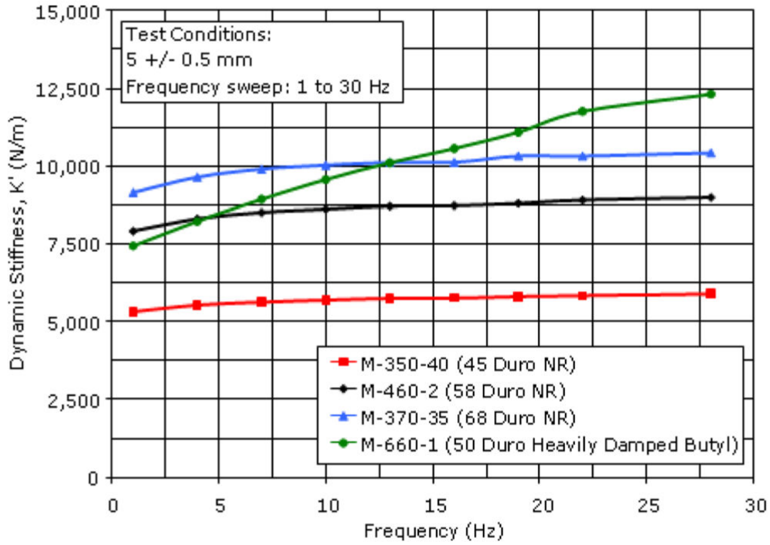

Fig. 13.

Dynamic axial stiffness, K′, vs. frequency.

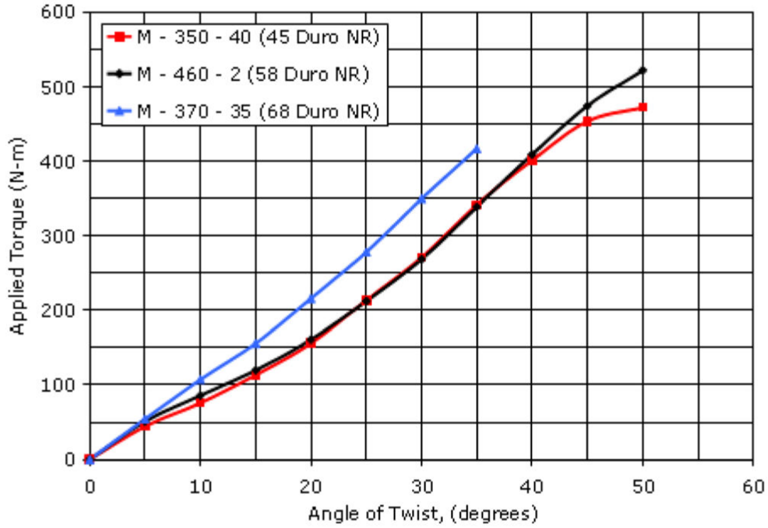

Fig. 14.

Torsion test, static torque vs. angle of twist.

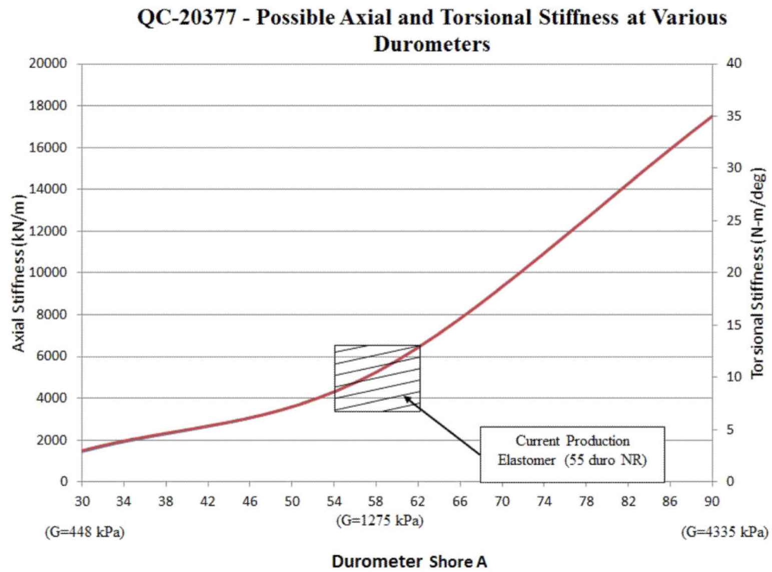

Fig. 15.

Locus of possible axial and torsion stiffness for production isolator bonded with various durometer elastomers.

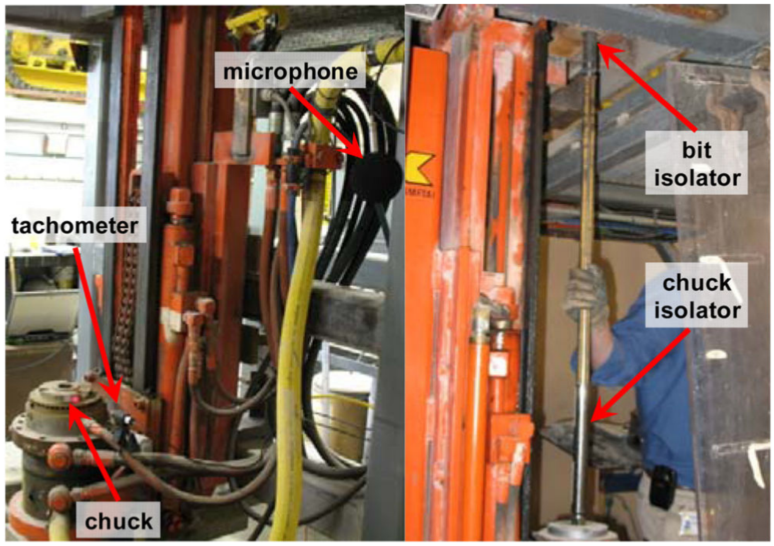

Fig. 16.

Test setup for sound level measurements at the operator's ear.

Author Manuscript
Author Manuscript
Author Manuscript

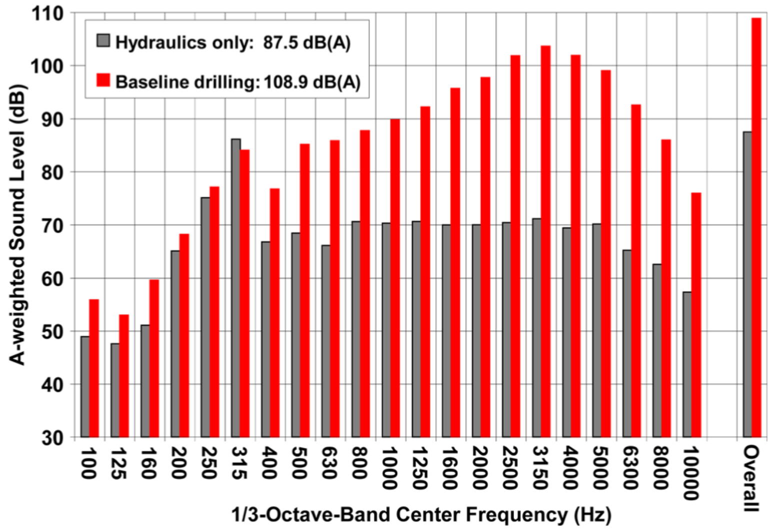

Fig. 17.

A-wtd SPL in 1/3-octave bands for hydraulics and baseline drilling conditions.

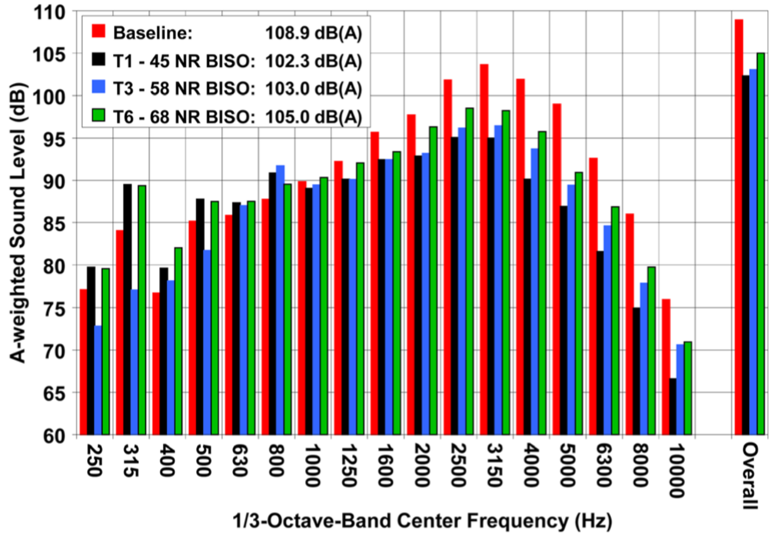

Fig. 18.

A-wtd SPL in 1/3-octave bands for baseline and with bit isolators.

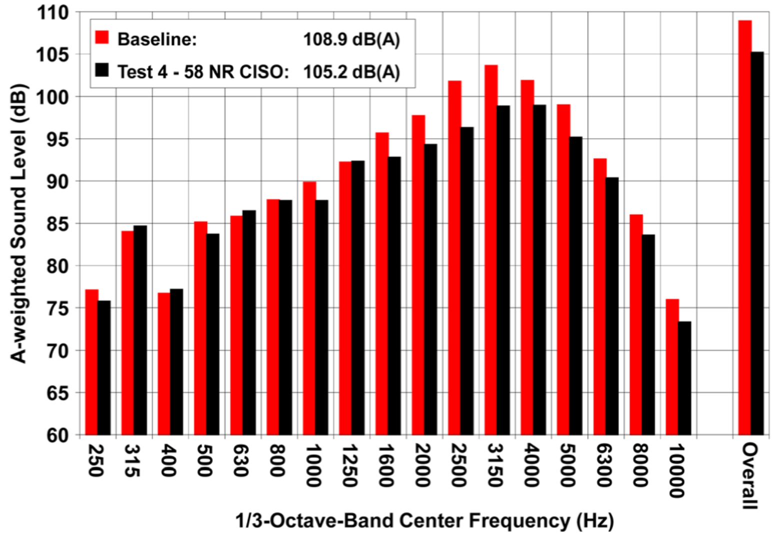

Fig. 19.

A-wtd SPL in 1/3-octave bands for baseline and with only a chuck isolator.

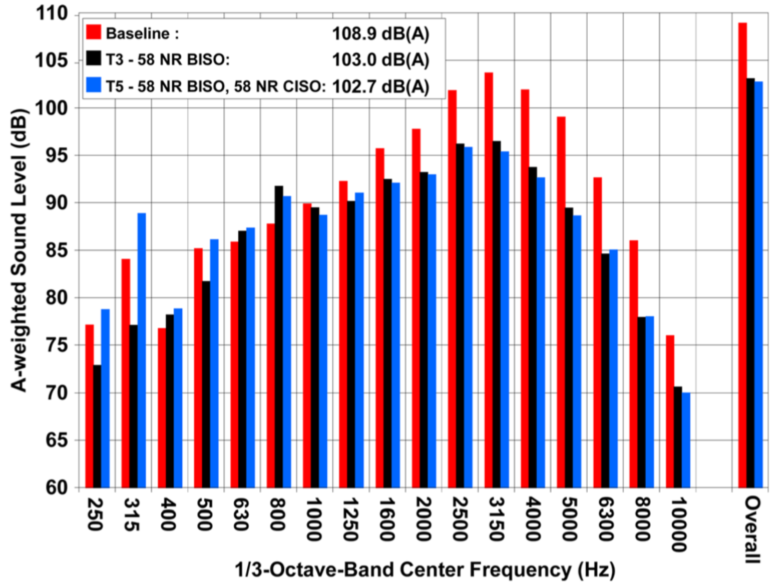

Fig. 20.

A-wtd SPL in 1/3-octave bands: baseline; 58 duro NR BISO; and 58 duro NR BISO with 58 duro NR CISO.

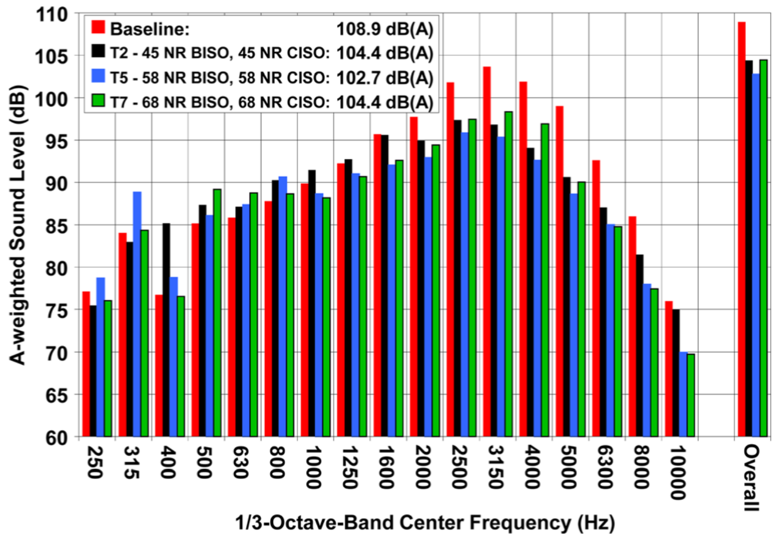

Fig. 21.

A-wtd SPL in 1/3-octave bands for baseline; 45 duro NR BISO and CISO; 58 duro NR BISO and CISO; and 68 duro NR BISO and CISO.

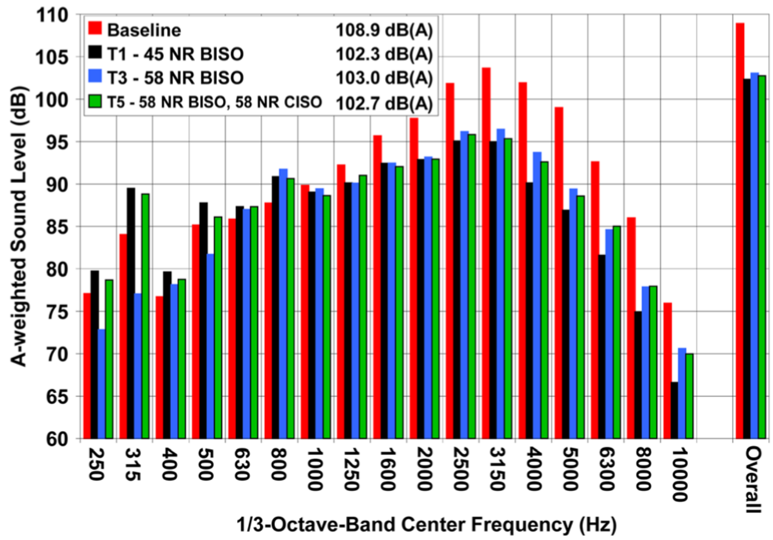

Fig. 22.

A-wtd SPL in 1/3-octave bands for baseline and best three tests: 45 duro NR BISO, 58 duro NR BISO, and 58 duro NR BISO with 58 duro NR CISO.

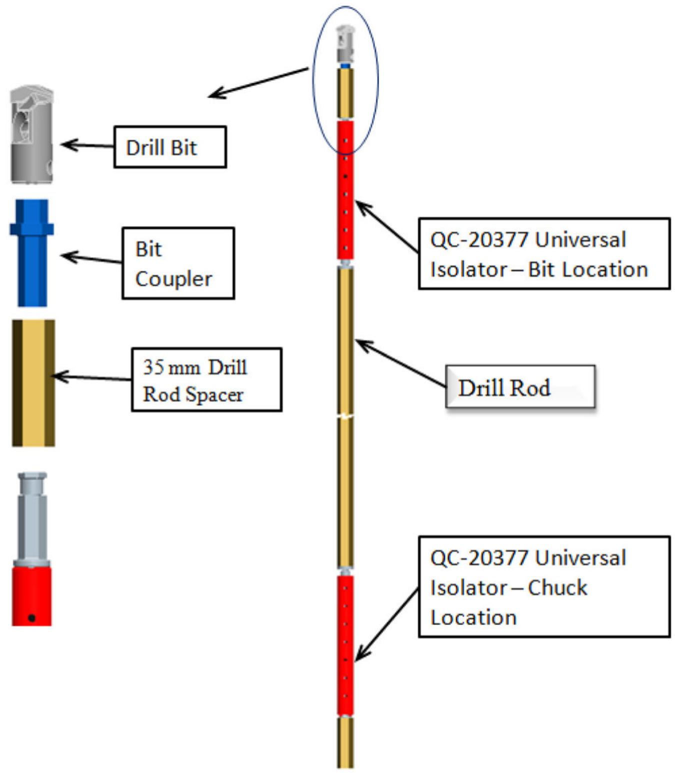

Fig. 23.

Second generation isolator (QC-20377) with male connections at both ends which can be installed into standard 35 mm drill rod.

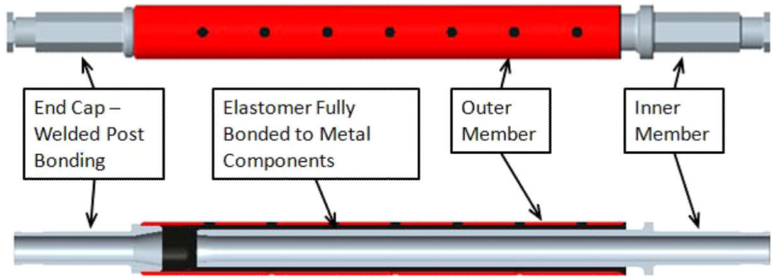

Fig. 24.
Cross section of second generation isolator (QC-20377).

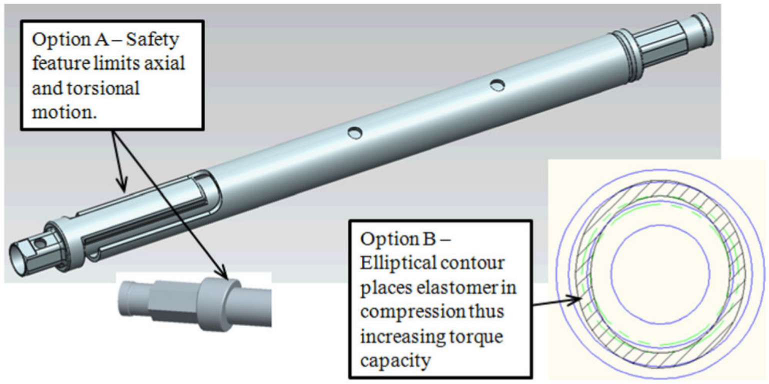

Fig. 25.
Other design options to increase load capacity and improve isolator life.

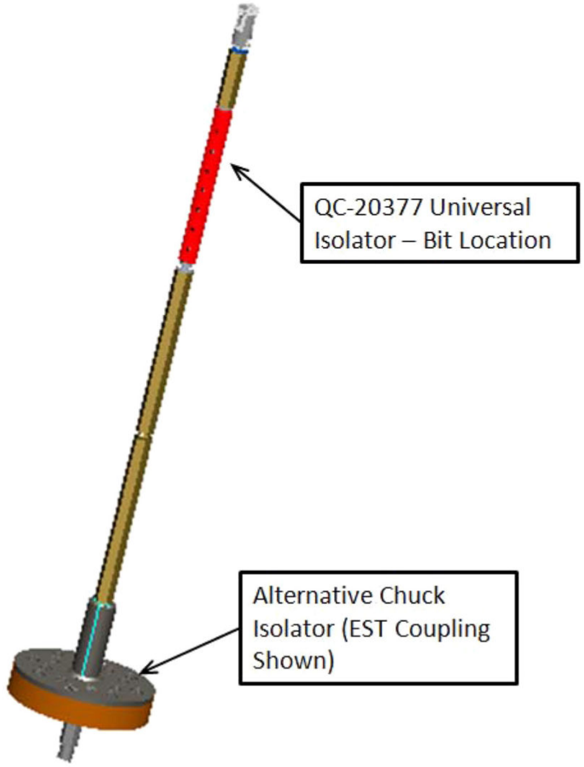

Fig. 26.

Alternative chuck isolator with standard QC-20377 drill bit isolator.

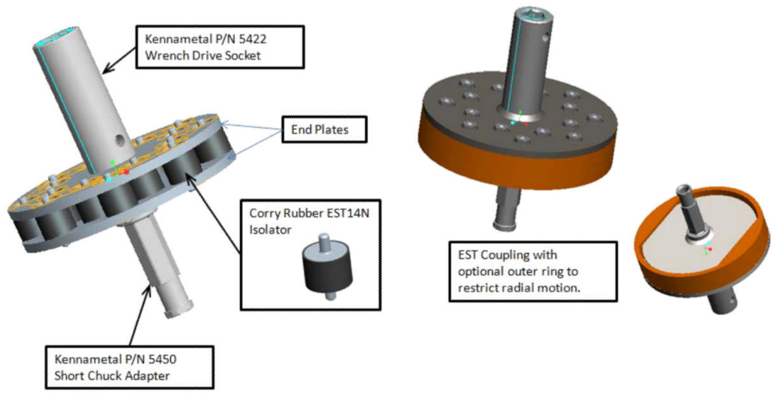

Fig. 27.

EST Chuck Isolator. This alternative chuck isolator design can be used for development. By adding/ subtracting isolators, stiffness can be adjusted to find optimal properties which then can be designed into a production version (alternatively this design can be used for short term production – no tooling required).

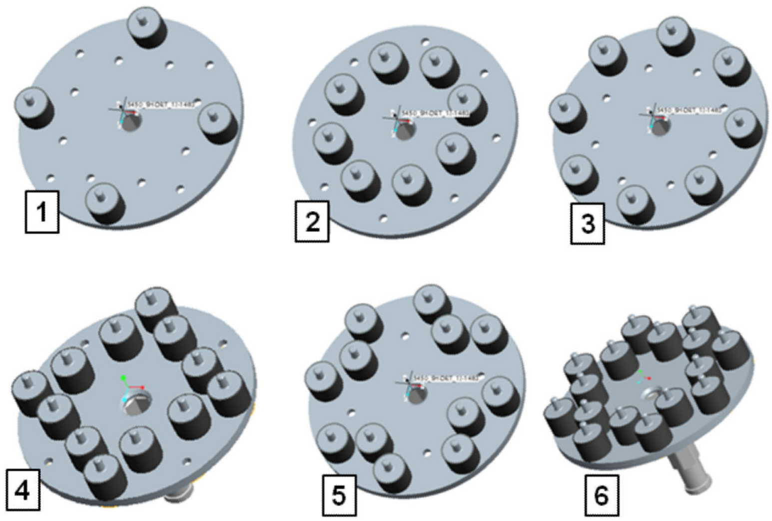

Fig. 28.
EST Chuck Isolator with possible configurations.

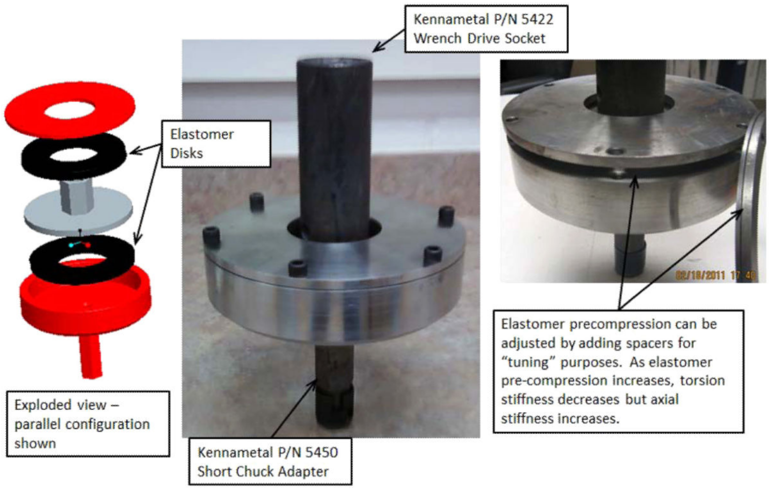

Fig. 29.

Pancake Chuck Isolator. This alternative chuck isolator design uses flat elastomeric disks. The size, durometer, arrangement (series or parallel) and pre-compression can all be modified to produce broad range of stiffness values.

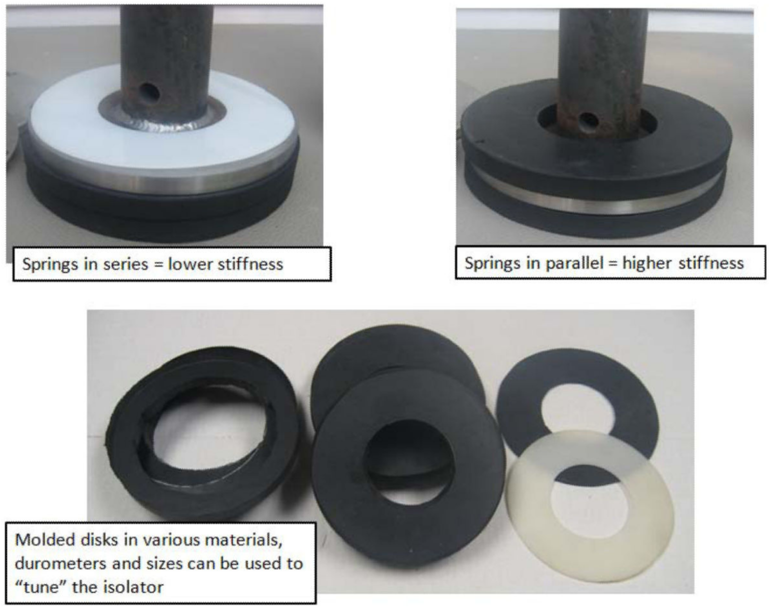

Fig. 30.

Molded disks used in pancake chuck isolator. The size, durometer and arrangement of these disks (i.e. parallel or series arrangement) and amount of pre-compression can greatly alter the stiffness of the coupling.

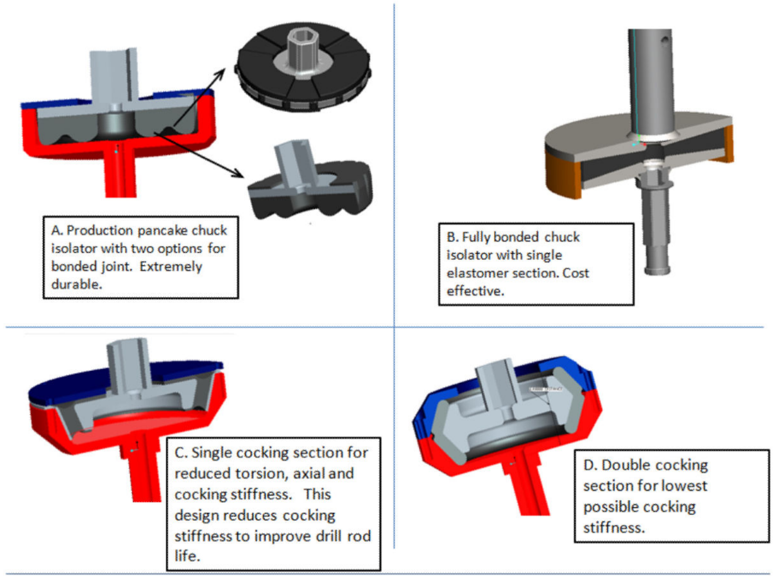

Fig. 31.

Possible production designs for chuck isolator. All these designs incorporate bonded elastomer for consistent stiffness. The appropriate configuration will be determined after testing is completed on the prototype chuck isolators.

Author Manuscript
Author Manuscript
Author Manuscript

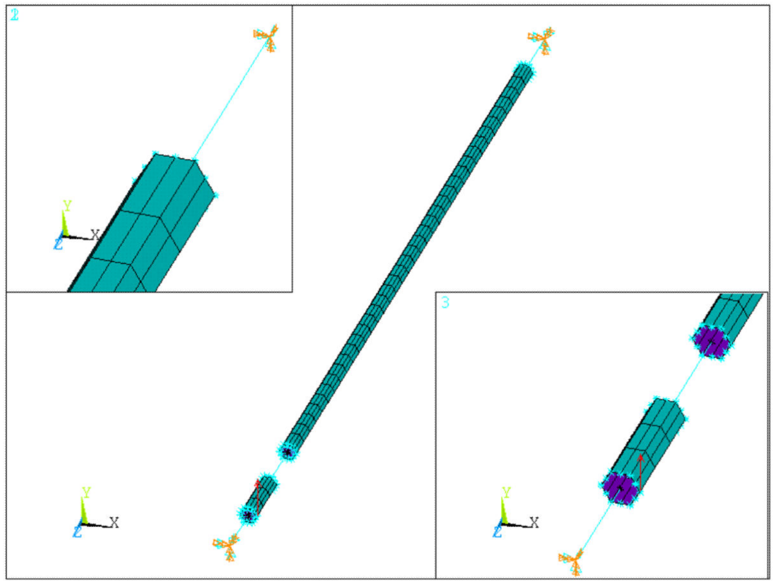

Fig. 32.
Model used in finite element analysis. 1.2 meter-long drill rod model with separate body to represent drill bit body. Fixed boundary conditions at chuck and at drilling media. Load can be FY (tangential) or FZ (axial), and is placed off-center on the drill bit tip, representing the drill bit cutting edge interaction with the drilling media (rock).

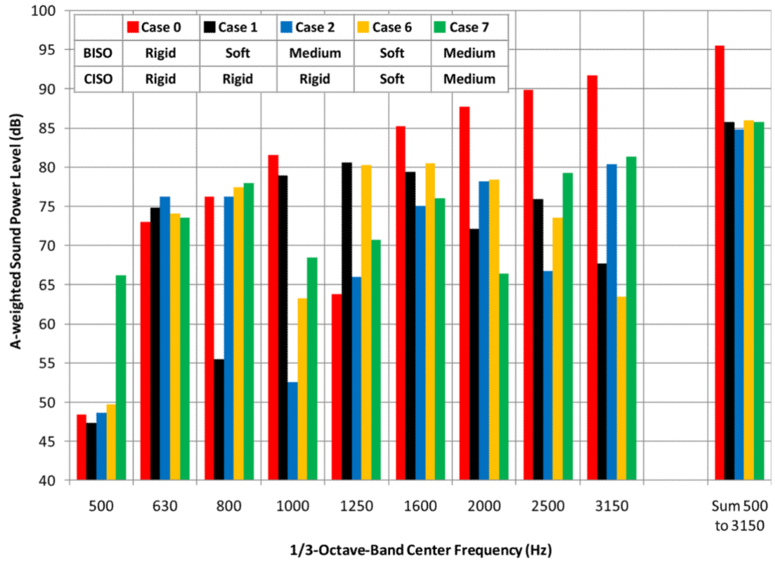

Fig. 33.

Estimated sound power level spectra for the 500 through 3150-Hz 1/3 octave bands for Cases 0, 1, 2, 6 and 7.

Table 1

Percentage of noise over-exposures by machine.

Machine	%
Continuous mining machine	35
Bull dozer	24
Roof bolting machine	17
Front end loader	8
Shuttle car	6
Auger miner	5
Truck	5

Table 2

Time spent by task minutes.

Task	Operator 1	Operator 2
Both drilling & bolting	218	218
Drilling alone	7	10
Riding mantrip	28	28
Tramming	63	63
Lunch	54	54
Prep time	108	108
Other	241	239

Table 3

PEL Dose by task, %.

Task	Operator 1	Operator 2
Both drilling & bolting	52	68
Drilling alone	2	4
Riding mantrip	8	21
Tramming	11	18
Lunch	0	2
Prep time	5	9
Other	0	7
Total	78	127

Table 4

Equivalent TWA sound level, dBA.

Task	Operator 1	Operator 2
Drilling	90	131
Bolting	70	86

Table 5

Evaluated elastomer compounds listed by CRC compound number and description.

100 Modulus (MPa)	Elongation (%)	Tensile (MPa)	Durometer (Shore A)	Damping Loss factor[A]
		M-350-40 : 45 durometer NR		
1.6	569	22.4	45.3	0.09
		M-460-2 : 58 durometer NR		
2.7	438	20.8	59.2	0.10
		M-370-35 : 68 durometer NR		
4.1	360	25.8	67.7	0.17
		M-660-1 : 50 durometer butyl rubber		
1.1	807	16.8	48.3	0.44

[A](tandel), 10 Hz ± 20% strain

Table 6

Stiffness results summary - Elastomers listed by compound number (CRC designation) and description.

Measured axial static (secant) stiffness at 7.6 mm (kN/m)	Measured axial static (secant) stiffness at 18 kN (kN/m)	Measured axial dynamic stiffness 10 Hz, ± 0.5 mm (kN/m)	Measured torsional (secant) stiffness at 410 N-m (N-m/deg)	Calculated cocking static stiffness (N-m/deg)	Calculated radial static stiffness (kN/m)
M-350-40 : 45 durometer NR					
4,000	2,900	5,400	8.9	2,750	38,650
M-460-2 : 58 durometer NR					
5,600	3,400	8,600	10.2	4,435	62,335
M-370-35 : 68 durometer NR					
6,100	4,000	10,200	11.9	6,210	87,270
M-660-1 : 50 durometer butyl rubber					
4,500	3,300	9,600	10.0	4,300	60,440

Table 7

Test configurations and results for sound level measurements.

TEST	BISO	CISO	Overall A-weighted Sound Level			
			Run 1	Run 2	AVG	Change vs Baseline
BG	NA	NA	48.1	NA	48.1	
HYD/VAC	NA	NA	87.4	NA	87.4	
BASE	NA	NA	108.2	109.3	108.8	
T1	45 Duro, NR	None	101.6	102.7	102.2	−6.6
T2	45 Duro, NR	45 Duro, NR	104.1	104.4	104.3	−4.5
T3	58 Duro, HR	None	102.9	NA	102.9	−5.9
T4	None	58 Duro, NR	104.7	105.4	105.1	−3.7
T5	58 Duro, NR	58 Duro, NR	101.9	103.2	102.6	−6.2
T6	68 Duro, NR	None	103.6	105.8	104.8	−3.9
T7	68 Duro, NR	68 Duro, NR	103.3	105.1	104.3	−4.5

Data collected w/rotation speed of 270 to 290 RPM, max thrust of 22 kN, feed rate of 28 mm/s. Baseline w/1.4 m long drill steel. BISO tests w/ 1.0 m long drill steel. CISO tests w/ 0.7 m long drill steel. Total length same (+/− 2.5 mm for all tests).

Author Manuscript

Author Manuscript

Author Manuscript

Table 8

Stiffness values of EST coupling for the various configurations shown in Fig. 28.

Configuration	K_{axial} (kN=m)	K_{radial} (kN/m)	$K_{torsion}$ (N-m/deg)	$K_{cocking}$ (N-m/deg)
1	350.4	105.1	15	28
2	700.8	189.2	16	45
3	700.8	189.2	31	86
4	1,051.20	283.8	32	73
5	1,051.20	283.8	39	114
6	1,401.60	378.4	47	130

Table 9

BISO and CISO stiffness and estimated sound power levels for each analysis case.

CASE	Isolator	Condition	Stiffness Axial (N/m)	Stiffness Torsional (N-m/rad)	Stiffness Cocking (N-m/rad)	Stiffness Radial (N/m)	Sound Power Level [dBA]
0	BISO	Rigid	175,100,000	58,275	8,547,000	2,057,425,000	95.6
	CISO	Rigid	175,100,000	58,275	8,547,000	2,057,425,000	
1	BISO	Soft	1,751,000	194	84,693	20,784,370	85.7
	CISO	Rigid	175,100,000	58,275	8,547,000	2,057,425,000	
2	BISO	Med	5,253,000	583	254,079	62,335,600	84.8
	CISO	Rigid	175,100,000	58,275	8,547,000	2,057,425,000	
3	BISO	Stiff	17,510,000	1,943	846,930	205,707,480	95.1
	CISO	Rigid	175,100,000	58,275	8,547,000	2,057,425,000	
4	BISO	Rigid	175,100,000	58,275	8,547,000	2,057,425,000	94.3
	CISO	Med	5,253,000	583	254,079	62,335,600	
5	BISO	Rigid	175,100,000	58,275	8,547,000	2,057,425,000	94.5
	CISO	Soft	1,751,000	194	84,693	20,784,370	
6	BISO	Soft	1,751,000	194	84,693	20,784,370	85.9
	CISO	Soft	1,751,000	194	84,693	20,784,370	
7	BISO	Med	5,253,000	583	254,079	62,335,600	85.7
	CISO	Med	5,253,000	583	254,079	62,335,600	
8	BISO	Med	5,253,000	583	254,079	62,335,600	85.8
	CISO	Soft	1,751,000	194	84,693	20,784,370	
9	BISO	Med	5,253,000	583	254,079	62,335,600	85.5
	CISO	Soft_C	1,751,000	194	777	17,510,000	
10	BISO	Med	5,253,000	583	254,079	62,335,600	85.1
	CISO	Soft_C_R	1,751,000	194	777	1,751,000	
11	BISO	Med	5,253,000	583	254,079	62,335,600	85.5
	CISO	Med_C	5,253,000	583	2,331	17,510,000	
12	BISO	Med	5,253,000	583	254,079	62,335,600	85.2
	CISO	Med_C_R	5,253,000	583	2,331	5,253,000	
13	BISO	Rigid	175,100,000	58,275	8,547,000	2,057,425,000	94.5
	CISO	Soft_C	1,751,000	194	777	17,510,000	
14	BISO	Rigid	175,100,000	58,275	8,547,000	2,057,425,000	95.8
	CISO	Soft_C_R	1,751,000	194	777	1,751,000	
15	BISO	Soft	1,751,000	194	84,693	20,784,370	86.0
	CISO	Soft_C	1,751,000	194	777	17,510,000	
16	BISO	Soft	1,751,000	194	84,693	20,784,370	85.9
	CISO	Soft_C_R	1,751,000	194	777	1,751,000	

Table 10

Validation of FEA Model by comparison to test data (from Table 7).

			FEA		TEST				
FEA Model CASE	**Isolator**	**Condition**	**Sound Power Level [dBA]**	**Delta vs. CASE 0**	**Test ID**	**Isolator**	**Condition**	**Sound Power Level [dBA]**	**Delta vs. Base**
0	BISO CISO	Rigid Rigid	95.6	-	Base	BISO CISO	None None	108.8	-
2	BISO CISO	Med Rigid	84.8	− 10.8	T3	BISO CISO	55 Duro, NR None	102.9	−5.9
4	BISO CISO	Rigid Med	94.3	− 1.3	T4	BISO CISO	None 55 Duro, NR	105.1	−3.7
7	BISO CISO	Med Med	85.7	−9.9	T5	BISO CISO	55 Duro, NR 55 Duro, NR	102.6	−6.2